Title

Structure-activity relationship studies of benzothiazole-phenyl analogs as multi-target ligands to alleviate pain without affecting normal behavior

Authors

Angelia, Jeannes
Weng, Xiaohui
Solomatov, Aleksei
et al.

Peer reviewed

Structure-activity relationship studies of benzothiazole-phenyl analogs as multi-target ligands to alleviate pain without affecting normal behavior

Jeannes Angelia[1], **Xiaohui Weng**[1], **Aleksei Solomatov**[1], **Christopher Chin**[2], **Alyssa Fernandez**[2], **Paula K. Hudson**[1], **Christophe Morisseau**[3], **Bruce D. Hammock**[3], **Ram Kandasamy**[2,*], **Stevan Pecic**[1,*]

[1]Department of Chemistry & Biochemistry, California State University, Fullerton, 800 N. State College, Fullerton, CA 92834, United States

[2]Department of Psychology, California State University, East Bay, 25800 Carlos Bee Blvd. Science S229, Hayward, CA 94542, United States

[3]Department of Entomology and Nematology, and UCD Comprehensive Cancer Center, University of California Davis, Davis, CA 95616, United States

Abstract

Soluble epoxide hydrolase (sEH) and fatty acid amide hydrolase (FAAH) are potential targets for several diseases. Previous studies have reported that concomitant selective inhibition of sEH and FAAH produced antinociception effects in an animal model of pain. However, the co-administration of a selective sEH inhibitor and a selective FAAH inhibitor might produce serious side effects due to drug-drug interactions that could complicate drug development in the long term. Thus, discovering dual sEH/FAAH inhibitors, single small molecules that can simultaneously inhibit both sEH and FAAH, would be a significant accomplishment in the medicinal chemistry field. Herein, we report the synthesis and biological evaluation of benzothiazole-phenyl-based analogs as potential dual sEH/FAAH inhibitors. This work represents a follow-up structure-activity relationship (SAR) and metabolic-stability studies of our best dual sEH/FAAH inhibitor identified previously, as well as *in vivo* evaluation of its effects on voluntary locomotor behavior in rats. Our SAR study indicates that trifluoromethyl groups on the aromatic rings are well tolerated by the targeted enzymes when placed at the *ortho* and *para* positions; however, they, surprisingly, did not improve metabolic stability in liver microsomes. Our behavioral studies indicate that doses of dual sEH/FAAH inhibitors that alleviate pain do not depress voluntary behavior in naïve rats, which is a common side effect of currently available analgesic drugs (e.g., opioids). Thus, dual sEH/FAAH inhibitors may be a safe and effective approach to treat pain.

*Corresponding authors. ram.kandasamy@csueastbay.edu (R. Kandasamy), specic@fullerton.edu (S. Pecic).

Declaration of Competing Interest

The authors declare that they have no known competing financial interests or personal relationships that could have appeared to influence the work reported in this paper.

Keywords

Structure-Activity Relationship study; Enzyme inhibition; Polypharmacology; Microwave-assisted synthesis; Molecular modeling; Microsomal liver stability assay; Wheel running; Locomotor activity

1   Introduction

Soluble epoxide hydrolase (sEH) regulates aliphatic epoxides of fatty acids,[1] among which are epoxyeicosatrienoic acids (EETs).[2] EETs are the epoxidation products of arachidonic acid by cytochrome P450s (CYP).[3, 4] sEH hydrolyzes the bioactive and anti-inflammatory EETs into its less bioactive and pro-inflammatory diol product, dihydroxyeicosatrienoic acids (DHETs)[5], Fig. 1. Therefore, inhibition of the sEH would lead to an elevated cellular concentration of EETs, which has promising therapeutic effects on pain, inflammation, and neurodegenerative diseases.[6, 7] To date, the most explored class of sEH inhibitors are urea-based compounds (e.g., t-TUCB, TPPU, Fig. 2)[5, 8]; however, many other structurally different sEH inhibitors are known to be potent sEH inhibitors, such as amides[9, 10], and aminobenzisoxazoles[11], represented with compounds **1** and **2**, respectively, in Fig. 2.

Fatty acid amide hydrolase (FAAH) is involved in the anandamide (AEA) signaling pathway. AEA and 2-arachidonoylglycerol (2-AG) are endogenous cannabinoid lipid ligands[12, 13], which activate the CB1 and CB2 G protein-coupled receptors in the mammalian endocannabinoid system.[14] FAAH hydrolyzes AEA into its inactive metabolites, arachidonic acid and ethanolamine, while monoacylglycerol lipase (MAGL) metabolizes 2-AG into arachidonic acid and glycerol, preventing CB1 and CB2 activation (Fig.1).[15] There has been a growing interest in developing FAAH inhibitors within the past few years.[16, 17] It has been associated with many therapeutical properties, including pain relief[18], anti-inflammatory effects[19], and mild anti-depressant[20] effects. Among a few FAAH inhibitors explored are urea-based inhibitors (URB 597), amides (e.g., **3**), and carbamate-based inhibitors (PF-750), Fig. 2.[15, 21]

Sasso et al. have shown that combinations of the sEH inhibitor TPPU and the FAAH inhibitor URB937 produced robust synergetic antinociception against carrageenan-induced acute inflammatory pain.[22] However, the co-administration of a selective sEH inhibitor and a selective FAAH inhibitor could not only lead to adverse effects due to the possibility of drug-drug interactions, but also to imbalanced dual treatment due to differential pharmacology of both compounds. Further, introducing several drugs may have adverse effects on normal behavior, but this is rarely assessed in animal studies of pain. Multi-targeted directed ligands, also known as polypharmacology, is a modern medicinal chemistry approach to designing a single bioactive molecule to interact with multiple targets.[23] Multitarget ligands can reduce side effects compared to drug combination therapy as well as reduce the time to determine the pharmacokinetic and pharmacodynamic properties of the drugs.[24] Therefore, we are developing dual sEH/FAAH inhibitors using the poly-pharmacological approach.

Toward this goal, our laboratory has recently discovered several benzothiazole-phenyl-based compounds that exhibit low nanomolar inhibition potencies for both sEH and FAAH enzymes, with the 2-chloro analog **4** being the most potent with IC_{50} values of 7 nM and 9.6 nM for human FAAH and human sEH enzymes, respectively (Fig. 2).[25] This dual inhibitor was shown to alleviate acute inflammatory pain in rats.[26] In fact, doses of this dual inhibitor are as effective as the traditional nonsteroidal anti-inflammatory drug ketoprofen.[26] However, an important step for drug discovery to treat pain is to ensure that therapeutic drug doses do not produce unwanted adverse effects related to normal behaviors. The pharmaceutical goal of pain relief is not only to eliminate discomfort, but also to ensure that normal activity is not affected. Thus, here, we expand on those previous studies by further investigating the role of various groups placed on the aromatic ring located at the right side (circled in red, Fig. 3) of the dual sEH/FAAH benzothiazole-phenyl scaffold; we tested **4** in mouse and rat sEH inhibition assays and performed liver metabolic stability assay. Lastly, we evaluated the behavioral effect of a dose (1 mg/kg) of inhibitor **4** that produces antinociception against inflammatory pain on the normal ability of uninjured male rats to voluntary run on a wheel to determine whether these doses produce locomotor side effects.

2 Experimental

2.1 Materials

All solvents and reagents were obtained from commercial suppliers, used without further purification, or prepared according to published procedures. Analytical thin-layer chromatography (TLC) was performed on aluminum plates precoated with silica gel, obtained from Sigma–Aldrich. Flash chromatography was carried out on the Teledyne CombiFlash Rf+ system using commercially available prepacked columns. Proton and carbon NMR spectra were recorded with a Bruker 400 MHz NMR spectrometer. Proton chemical shifts are reported relative to the residual solvent peak (chloroform = 7.26 ppm or dimethyl sulfoxide = 2.50 ppm) as follows: chemical shift (δ), proton ID, multiplicity (s = singlet, bs = broad singlet, d = doublet, bd = broad doublet, dd = doublet of doublets, t = triplet, q = quartet, m = multiplet, integration, coupling constant(s) in Hz). Carbon chemical shifts are reported relative to the residual deuterated solvent signals (chloroform = 77.2 ppm, or dimethyl sulfoxide = 39.5 ppm). All compounds described were of >95% purity. Purity was confirmed by a high-resolution liquid chromatography-mass spectrometer (ThermoFisher Scientific system). Elution was isocratic with water (30%, +0.1% formic acid) and acetonitrile (70%, +0.1% formic acid) at a flow rate of 0.4 mL/min. For compounds containing chlorine and/or bromine, ^{35}Cl and ^{79}Br isotopes were measured, respectively. Microwave reactions were carried out in a CEM 2.0 Discover microwave synthesizer. Melting points were measured with a MEL-TEMP II melting point apparatus and are reported uncorrected. Human recombinant FAAH enzyme (Item No. 100101183, Batch No. 0523867) and human recombinant sEH enzyme (Item No. 10011669) was obtained from Cayman Chemical. Fig. 1 was created with BioRender.com. Molecular modeling studies and docking experiments were performed using ICM Pro Molsoft software.

2.2   Chemistry

General procedure for the preparation of benzothiazole-phenyl analogs—The mixture of *N*-Boc-4-piperidine carboxylic acid (500 mg, 2.18 mmol), 2-(4-aminophenyl) benzothiazole (493 mg, 2.18 mmol), 1-ethyl-3-(3-dimethylaminopropyl)carbodiimide, EDC (504 mg, 2.62 mmol) and a catalytic amount of 4-dimethylamino pyridine, DMAP, were dissolved in anhydrous dichloromethane, DCM (20 mL). The reaction mixture was subjected to microwave irradiation at 80 °C for 20 min. The mixture was transferred to a separatory funnel, and the organic layer was washed with an aqueous solution of 1M hydrochloric acid (20 mL), an aqueous solution of saturated sodium bicarbonate $NaHCO_3$ (15 mL), and brine (20 mL). The organic layer was then dried over anhydrous sodium sulfate, filtered, and concentrated. The crude product was purified by column chromatography (CombiFlash system, 0-50% ethyl acetate/hexane), and **3** was obtained as a white solid, 728 mg, 76%: mp: 238–240 °C. ^{1}H NMR (400 MHz, CDCl$_3$) δ ppm 8.05 – 8.02 (m, 3H), 7.88 (d, J = 7.2 Hz, 1H), 7.67 (d, J = 8.4 Hz, 2H), 7.62 (s, 1H), 7.47 (t, J = 7.2 Hz, 1H), 7.36 (t, J = 6.8 Hz, 1H), 4.17 (bs, 1H), 2.77 (t, J = 11.2 Hz, 2H), 2.43 – 2.37 (m, 1H), 1.89 (d, J = 10.8 Hz, 2H), 1.79 – 1.70 (m, 3H), 1.47 (s, 9H). ^{13}C NMR (100 MHz, CDCl$_3$) δ 172.9, 167.5, 154.8, 154.2, 140.4, 135.0, 129.6, 128.5, 126.4, 125.2, 123.1, 121.7, 119.9, 79.9, 44.5, 28.7, 28.5 ppm. Next, **3** (500 mg, 1.14 mmol) was dissolved in anhydrous DCM (15 mL), stirred in an ice bath at 0 °C, and trifluoroacetic acid, TFA (1 mL, 11.4 mmol) was added dropwise into the solution. The reaction mixture was stirred at room temperature for 18 hours under an argon atmosphere. Reaction progress was monitored by TLC until a single spot was achieved. After concentration *in vacuo*, the crude product was triturated with diethyl ether and filtered. Product **4** was obtained as a TFA salt, pale green solid, yielding 90% (0.9 mmol, 345 mg) and used for the next step without further purification. A small amount was free-based and used for NMR analysis: mp: 242–244 °C. ^{1}H NMR (400 MHz, DMSO-*d$_6$*) δ ppm 10.31 (s, 1H), 8.11 (d, *J* = 8 Hz, 1H), 8.02 (t, *J* = 9.2 Hz, 3H), 7.81 (d, *J* = 8.8 Hz, 2H), 7.52 (t, *J* = 8.4 Hz, 1H), 7.43 (t, *J* = 8 Hz, 1H), 4.23 (bs, 1H), 3.14 (d, *J* = 12.4 Hz, 2H), 2.68 (t, *J* = 12.4 Hz, 2H), 2.59 – 2.55 (m, 1H), 1.82 (d, *J* = 11.6 Hz, 2H), 1.65 (q, *J* = 12, 11.6 Hz, 2H). ^{13}C NMR (100 MHz, DMSO-*d$_6$*) δ 173.5, 166.9, 153.6, 142.1, 134.2, 127.9, 127.4, 126.5, 125.2, 122.5, 122.2, 119.3, 44.1, 42.1, 27.5 ppm. *N*-(4-(benzo[d]thiazol-2-yl)phenyl)piperidine-4-carboxamide **4,** as a TFA salt (100 mg, 0.22 mmol) and corresponding benzenesulfonyl chloride (0.22 mmol), were dissolved in anhydrous DCM (20 mL). Triethylamine (0.15 mL, 1.1 mmol) was added, and the reaction mixture was subjected to microwave irradiation at 80 °C for 20 min. Next, the mixture was transferred to a separatory funnel, where the organic layer was washed with an aqueous solution of saturated $NaHCO_3$ (20 mL). The organic layer was dried over anhydrous sodium sulfate, filtered, and concentrated. The crude product was purified by column chromatography (CombiFlash system, 0-100% ethyl acetate/hexane)) and recrystallized from diethyl ether.

N-(4-(benzo[d]thiazol-2-yl)phenyl)-1-((2-(trifluoromethyl)phenyl)sulfonyl)piperidine-4-carboxamide, **7a** was obtained as an off-white solid in the amount of 62 mg (51% yield), mp: 237-239 °C. ^{1}H NMR (400 MHz, DMSO-*d$_6$*) δ 10.26 (s, 1H), 8.13-7.88 (m, 8H), 7.81-7.78 (m, 2H), 7.55-7.41 (m, 2H), 3.79-3.76 (m, 2H), 2.85 (td, *J* = 12.3, 2.2 Hz, 2H), 1.94-1.90 (m, 2H), 1.70-1.59 (m, 2H). ^{13}C NMR (100 MHz,

DMSO-d_6): δ 173.5, 167.4, 154.1, 142.5, 137.90, 137.89, 134.7, 133.94, 133.90, 131.7, 129.17, 129.11, 128.4, 128.0, 127.0, 126.5, 125.7, 123.0, 122.7, 121.8, 119.9, 45.2, 42.1, 28.5 ppm. HRMS-ESI+: calculated for $C_{26}H_{22}F_3N_3O_3S_2$ + H = 546.1127; Found: 546.1122.

N-(4-(benzo[d]thiazol-2-yl)phenyl)-1-((2-cyanophenyl)sulfonyl)piperidine-4-carboxamide, **7b** was obtained as a white solid in the amount of 78 mg (71% yield), mp: 212–213 °C. ^{1}H NMR (400 MHz, DMSO-d_6) δ 10.22 (s, 1H), 8.20-8.17 (m, 1H), 8.12-7.91 (m, 7H), 7.79-7.76 (m, 2H), 7.52 (ddd, J = 8.2, 7.1, 1.2 Hz, 1H), 7.43 (ddd, J = 8.1, 7.1, 1.1 Hz, 1H), 3.79 (d, J = 12.5 Hz, 2H), 2.77-2.71 (m, 2H), 2.48-2.45 (m, 1H), 1.94-1.90 (m, 2H), 1.68-1.62 (m, 2H). ^{13}C NMR (100 MHz, DMSO-d_6): δ 173.4, 167.4, 154.1, 142.4, 139.6, 136.7, 134.7, 134.5, 134.1, 130.6, 128.4, 128.0, 127.0, 125.7, 123.0, 122.7, 119.8, 116.8, 109.9, 45.4, 41.9, 28.1 ppm. HRMS-ESI+: calculated for $C_{26}H_{22}N_4O_3S_2$ + H = 503.1206; Found: 503.1202.

N-(4-(benzo[d]thiazol-2-yl)phenyl)-1-((3-(trifluoromethyl)phenyl)sulfonyl)piperidine-4-carboxamide, **7c** was obtained as an off-white solid in the amount of 48 mg (40% yield), mp: >250 °C. ^{1}H NMR (400 MHz, DMSO-d_6) δ 10.16 (s, 1H), 8.16-7.92 (m, 8H), 7.76 (d, J = 8.9 Hz, 2H), 7.52 (ddd, J = 8.2, 7.1, 1.2 Hz, 1H), 7.43 (ddd, J = 8.1, 7.1, 1.1 Hz, 1H), 3.77-3.74 (m, 2H), 2.48-2.36 (m, 1H), 1.94-1.90 (m, 2H), 1.71-1.60 (m, 2H). ^{13}C NMR (100 MHz, DMSO-d_6): δ 173.4, 167.4, 154.1, 142.4, 137.7, 134.7, 131.7, 128.4, 128.0, 127.0, 125.7, 123.0, 122.7, 119.8, 45.7, 41.8, 28.0 ppm. HRMS-ESI+: calculated for $C_{26}H_{22}F_3N_3O_3S_2$ + H = 546.1127; Found: 546.1122.

N-(4-(benzo[d]thiazol-2-yl)phenyl)-1-((4-(trifluoromethyl)phenyl)sulfonyl)piperidine-4-carboxamide, **7d** was obtained as a white solid in the amount of 55 mg (46% yield), mp: >250 °C. ^{1}H NMR (400 MHz, DMSO-d_6) δ 10.16 (s, 1H), 8.13-8.00 (m, 8H), 7.78-7.76 (m, 2H), 7.52 (ddd, J = 8.2, 7.1, 1.2 Hz, 1H), 7.43 (ddd, J = 8.1, 7.1, 1.1 Hz, 1H), 3.72 (d, J = 12.0 Hz, 2H), 2.46-2.41 (m, 1H), 1.94-1.89 (m, 2H), 1.69-1.65 (m, 2H). ^{13}C NMR (100 MHz, DMSO-d_6): δ 173.4, 167.4, 154.1, 142.4, 134.7, 128.9, 128.4, 128.0, 127.11, 127.07, 127.03, 125.7, 123.0, 122.7, 119.8, 45.7, 41.8, 28.0 ppm. HRMS-ESI+: calculated for $C_{26}H_{22}F_3N_3O_3S_2$ + H = 546.1127; Found: 546.1125.

N-(4-(benzo[d]thiazol-2-yl)phenyl)-1-((4-nitrophenyl)sulfonyl)piperidine-4-carboxamide, **7e** was obtained as an off-white solid in the amount of 58 mg (50% yield), mp: >250 °C. ^{1}H NMR (400 MHz, DMSO-d_6) δ 10.20 (s, 1H), 8.47-8.44 (m, 2H), 8.12-7.99 (m, 6H), 7.78-7.75 (m, 2H), 7.52 (ddd, J = 8.2, 7.2, 1.1 Hz, 1H), 7.43 (td, J = 7.6, 1.0 Hz, 1H), 3.73 (d, J = 11.8 Hz, 2H), 2.42-2.38 (m, 1H), 1.94-1.90 (m, 2H), 1.70-1.62 (m, 2H). ^{13}C NMR (100 MHz, DMSO-d_6): δ 173.4, 167.4, 154.1, 150.5, 142.4, 142.1, 134.7, 129.4, 128.4, 128.0, 127.0, 125.7, 125.2, 123.0, 122.7, 119.8, 45.6, 41.7, 28.0 ppm. HRMS-ESI+: calculated for $C_{25}H_{22}N_4O_5S_2$ + H = 523.1104; Found: 523.1103.

N-(4-(benzo[d]thiazol-2-yl)phenyl)-1-((2-chloro-4-fluorophenyl)sulfonyl)piperidine-4-carboxamide, **7f** was obtained as an off-white solid in the amount of 71 mg (61% yield), mp: >250 °C. ^{1}H NMR (400 MHz, DMSO-d_6) δ 10.25 (s, 1H), 8.12-8.00 (m, 5H), 7.80-7.76 (m, 3H), 7.54-7.41 (m, 3H), 3.76 (d, J = 12.7 Hz, 1H), 2.88-2.82 (m, 2H), 2.52-2,48 (dt, J = 3.7, 1.9 Hz, 1H), 1.92-1.87 (m, 2H), 1.67-1.58 (m, 2H). ^{13}C NMR (100 MHz, DMSO-d_6):

δ 173.5, 167.4, 165.7, 163.2, 154.1, 142.5, 134.7, 134.46, 134.36, 133.3, 133.07, 133.03, 128.4, 128.0, 127.0, 125.7, 123.0, 122.7, 120.4, 120.1, 119.8, 115.6, 115.4, 45.1, 42.1, 28.4 ppm. HRMS-ESI+: calculated for $C_{25}H_{21}ClFN_3O_3S_2$ + H = 530.0770; Found: 530.0767.

N-(4-(benzo[d]thiazol-2-yl)phenyl)-1-((2-chloro-4-(trifluoromethyl)phenyl)sulfonyl) piperidine-4-carboxamide, **7g** was obtained as a gray solid in the amount of 70 mg (55% yield), mp: >250 °C. ^{1}H NMR (400 MHz, DMSO-d_6) δ 10.26 (s, 1H), 8.23-7.95 (m, 7H), 7.79 (d, J = 8.8 Hz, 2H), 7.55-7.51 (m, 1H), 7.45-7.41 (m, 1H), 3.82-3.79 (m, 2H), 2.96-2.90 (m, 2H), 2.57-2.52 (m, 1H), 1.93-1.89 (m, 2H), 1.69-1.58 (m, 2H). ^{13}C NMR (100 MHz, DMSO-d_6): δ 173.5, 167.4, 154.1, 142.5, 140.5, 134.7, 133.0, 132.6, 128.4, 128.0, 127.0, 123.0, 122.7, 119.9, 45.2, 42.1, 28.5 ppm. HRMS-ESI+: calculated for $C_{26}H_{21}ClF_3N_3O_3S_2$ + H = 580.0738; Found: 580.0733.

N-(4-(benzo[d]thiazol-2-yl)phenyl)-1-((2-bromo-4-fluorophenyl)sulfonyl)piperidine-4-carboxamide, **7h** was obtained as a white solid in the amount of 63 mg (49% yield), mp: >250 °C. ^{1}H NMR (400 MHz, DMSO-d_6) δ 10.26 (s, 1H), 8.12-8.08 (m, 2H), 8.05-8.00 (m, 3H), 7.92 (dd, J = 8.5, 2.6 Hz, 1H), 7.80-7.78 (m, 2H), 7.54-7.41 (m, 3H), 3.75 (d, J = 12.8 Hz, 2H), 2.90-2.84 (m, 2H), 2.57-2.54 (m, 1H), 1.91-1.87 (m, 2H), 1.69-1.59 (m, 2H). ^{13}C NMR (100 MHz, DMSO-d_6): δ 173.5, 167.4, 165.4, 162.8, 154.1, 142.5, 134.72, 134.69, 134.65, 134.56, 134.46, 128.4, 128.0, 127.0, 125.7, 123.7, 123.4, 123.0, 122.7, 121.67, 121.56, 119.8, 115.9, 115.7, 45.1, 42.2, 28.4 ppm. HRMS-ESI+: calculated for $C_{25}H_{21}BrFN_3O_3S_2$ + H = 574.0265; Found: 574.0262.

N-(4-(benzo[d]thiazol-2-yl)phenyl)-1-((3-bromo-5-chlorophenyl)sulfonyl)piperidine-4-carboxamide, **7i** was obtained as an off-white solid in the amount of 79 mg (60% yield), mp: >250 °C. ^{1}H NMR (400 MHz, DMSO-d_6) δ 10.25 (s, 1H), 8.12-8.00 (m, 5H), 7.91 (d, J = 8.5 Hz, 1H), 7.80-7.78 (m, 3H), 7.54-7.50 (m, 1H), 7.44-7.40 (m, 1H), 3.77-3.74 (m, 2H), 2.89-2.83 (m, 2H), 2.54-2.52 (m, 1H), 1.91-1.88 (m, 2H), 1.66-1.57 (m, 2H). ^{13}C NMR (400 MHz, DMSO-d_6): δ 173.5, 167.4, 154.1, 142.5, 135.8, 134.90, 134.72, 133.4, 132.6, 131.4, 128.4, 128.0, 127.7, 127.0, 125.7, 123.0, 122.7, 119.8, 45.1, 42.1, 28.5 ppm. HRMS-ESI+: calculated for $C_{25}H_{21}BrClN_3O_3S_2$ + H = 589.9969; Found: 589.9967.

N-(4-(benzo[d]thiazol-2-yl)phenyl)-1-((3,5-bis(trifluoromethyl)phenyl)sulfonyl)piperidine-4-carboxamide, **7j** was obtained as a gray solid in the amount of 85 mg (63% yield), mp: >250 °C. ^{1}H NMR (400 MHz, DMSO-d_6) δ 10.16 (s, 1H), 8.58 (s, 1H), 8.35 (s, 2H), 8.11 (dd, J = 8.0, 0.6 Hz, 1H), 8.01 (dd, J = 8.4, 6.8 Hz, 3H), 7.77 (d, J = 8.8 Hz, 2H), 7.52 (td, J = 7.7, 1.1 Hz, 1H), 7.42 (td, J = 7.6, 1.1 Hz, 1H), 3.83 (d, J = 12.1 Hz, 2H), 2.44-2.38 (m, 1H), 1.95-1.91 (m, 2H), 1.70-1.60 (m, 2H).^{13}C NMR (400 MHz, DMSO-d_6): δ 173.3, 167.4, 154.1, 142.4, 139.5, 134.7, 132.3, 132.0, 128.41, 128.38, 128.0, 127.0, 125.7, 124.4, 123.0, 122.7, 121.7, 119.8, 45.6, 41.7, 28.0 ppm. HRMS-ESI+: calculated for $C_{27}H_{21}F_6N_3O_3S_2$ + H = 614.1001; Found: 614.0996.

N-(4-(benzo[d]thiazol-2-yl)phenyl)-1-((4-bromo-2,6-dichlorophenyl)sulfonyl)piperidine-4-carboxamide, **7k** was obtained as an off-white solid in the amount of 63 mg (46% yield), mp: >250 °C. ^{1}H NMR (400 MHz, DMSO-d_6) δ 10.27 (s, 1H), 8.12-7.99 (m, 5H), 7.82-7.76 (m, 2H), 7.62-7.49 (m, 1H), 7.45-7.40 (m, 1H), 3.84-3.81 (m, 2H),

3.00-2.94 (m, 2H), 2.60-2.54 (m, 1H), 1.92-1.87 (m, 2H), 1.66-1.56 (m, 2H). ^{13}C NMR (400 MHz, DMSO-d_6): δ 173.5, 154.1, 142.5, 135.8, 134.7, 132.4, 128.4, 128.0, 127.0, 126.7, 125.7, 123.0, 122.7, 119.8, 100.0, 45.0, 42.1, 28.4 ppm. HRMS-ESI+: calculated for $C_{25}H_{20}BrCl_2N_3O_3S_2$ + H = 623.9579; Found: 623.9578.

2.3 Biological evaluation

Experimental details for the quantification of inhibitor potencies have been previously published for both FAAH[21] and sEH[25] enzymes. In brief, fluorescence generated by hydrolysis was quantified every 30 seconds for 10 min, and the linear portion of the curve was used to generate the reaction velocity ($v_{inhibitor}$). Values were subtracted from wells containing no enzyme. Next, the IC_{50} values were quantified by simple linear regression of the log [I] vs. % remaining activity ($v_{inhibitor}/v_{DMSO}$) and determining x when y = 0.50. All measurements were the average of triplicates. For all assays, the final DMSO concentration was 2%.

sEH Inhibition Assay: The substrate cyano(6-methoxynaphthalen-2-yl)methyl((3-phenyloxiran-2-yl)methyl)carbonate (CMNPC) ($[S]_{final}$ = 5 μM) was added to wells containing human/mouse/rat sEH in sodium phosphate buffer [0.1 M, pH = 7.4 and 0.1 mg/mL bovine serum albumin (BSA)], and formation of the fluorescent 6-methoxynaphthaldehyde ($\lambda_{excitation}$ = 330 nm, $\lambda_{emission}$ = 465 nm, 30 °C) was measured by the use of a microplate reader (Molecular Devices., CA, USA).

FAAH Inhibition Assay: Measurement of human FAAH potency was performed using the substrate N-(6-methoxypyridin-3-yl) octanamide (OMP) ($[S]_{final}$ = 50 μM) in sodium phosphate buffer (0.1 M, pH = 8, 0.1 mg/mL BSA). Progress of the reaction was measured by fluorescence detection of 6-methoxypyridin-3-amine at an excitation wavelength of 303 nm and an emission wavelength of 394 nm at 37 °C by the use of a microplate reader (Molecular Devices., CA, USA). The substrate, OMP, was synthesized following a previously reported synthetic procedure and reaction conditions.[21]

2.4 *In vitro* human liver microsomal metabolic stability

Microsomal liver stability assay was performed in mixed-gender rat liver microsomes (Xenotech) and human microsomes from the liver (Sigma Aldrich). In short, the test compound (final concentration of 1 μM) was incubated with the microsomes in a 100 mM phosphate buffer (pH=7.4) at 37 °C for 60 min for both human and rat microsomal assays. The reaction was initiated by adding an NADPH regenerating system containing glucose 6-phosphate, glucose 6-phosphate dehydrogenase, NADPH, and $MgCl_2$ (Sigma, St. Louis, MO) in phosphate buffer. Positive control incubations proceeded with testosterone as the substrate separately. Aliquots (100 μL) were withdrawn at 0, 10, 30, and 60 for human and rat microsomal assays. Reactions were terminated by adding methanol. The mixtures were centrifuged (13,500 rpm for 5 min), and the supernatants were evaporated. The residues were reconstituted in the mobile phase (500 uM, 50% acetonitrile, and 50% water, containing 0.1% formic acid and standard internal 7-ethoxycoumarin) and subjected to LC/MS analysis. The peak area response ratio (PARR) to internal standard was compared

to the PARR at time 0 to determine the percent remaining at each time point. Half-lives were calculated using GraphPad software, fitting to a single-phase exponential decay equation.[27]

2.5 Molecular modeling

Docking experiments and ADMET predictions were performed using the ICM Pro and ICM Chemist software.[28-30] For docking studies of t-TUCB, URB 597, and analogs **5a-k** were used, a crystal structure of human sEH complexed with *N*-cycloheptyl-1-(mesitylsulfonyl)piperidine-4-carboxamide (PDB file: 4HAI)[31] and a homology model of human FAAH enzyme[21]. For the docking experiments in the human sEH enzyme, the PDB: 4HAI was converted to an ICM file and optimized according to the program settings. Next, the inhibitor, *N*-cycloheptyl-1-(mesitylsulfonyl) piperidine-4-carboxamide, was removed, and binding pockets were identified. Docking experiments were performed following the program guidelines. FAAH homology model was previously validated and optimized[21] and used directly for docking experiments. ICM scores were obtained after this procedure. ADMET properties for all synthesized target analogs were calculated using the ICM Chemist Pro program guidelines.

2.6 *In vivo* evaluation of voluntary wheel running

Subjects: Data were collected from male Sprague-Dawley rats purchased from Charles River (Hollister, CA, USA) and housed at California State University, East Bay (Hayward, CA, USA). All rats were at least 40 days old at the start of the study and randomly assigned to treatment groups. Procedures were approved by the Institutional Animal Care and Use Committee of California State University, East Bay. All animals had access to food and water *ad libitum* and were only removed the cages once a day to administer drug or perform animal husbandry. All animals were housed in a room on a 12:12 light:dark cycle (lights off at 9 am).

Drugs: 4 was dissolved in vehicle (20% DMSO, 20% cremophor, and 60% saline). Drugs were injected intraperitoneally using a 26-gauge needle.

Wheel running: Animals were housed in standard Plexiglas rat cages containing metal running wheels (33 cm diameter; Tecniplast Rat Running Wheel, Starr Life Sciences). The running wheels were connected to a computer containing VitalView® Activity software to count the number of wheel revolutions. The number of wheel revolutions were collected in 5 min bins. Rats were allowed to habituate to the running wheel cages for 7 days before data collection. The number of wheel revolutions that occurred during 23 hours on the 8th day injection was used as the baseline measure. Experimental manipulations began the day after baseline assessment. On this day, rats were removed from their cages and weighed. Either **4** or vehicle was administered via intraperitoneal injection and rats were immediately returned to their cages to run. All injections occurred immediately prior to the beginning of the dark phase (9 am) to ensure that the drug's effect on behavior was captured. This procedure was repeated in a counterbalanced manner such that each rat was only treated once in one condition, and only half of the rats received an injection of **4** on each test day. No experimenters were in the room as wheel running data were collected.

Statistical Analysis: An average hourly nighttime running rate on Day 8 was used as the baseline for hour-by-hour analysis. All wheel running data are presented as a percent change from each rat's baseline value given individual differences in the magnitude of wheel running. Data were collected for the first two hours following drug injection. These levels of running were averaged across the two hours and compared. All data are expressed as mean ± SEM. Data were analyzed with one-way ANOVA. Statistical significance was defined as $p < 0.05$.

3   Results and Discussion

3.1   Design and Synthesis

The starting point for designing this series of dual inhibitors targeting FAAH and sEH enzymes was compound **4**, which was discovered in our previous work.[26] In short, we have shown that benzothiazole-phenyl moiety, connected with the amide-piperidine to the aromatic ring via sulfonamide bond, is essential for the dual inhibition, Fig. 3. The placement of fluoro-, chloro-, bromo-, methyl-, or methoxy- groups in the *ortho* position of the aromatic ring on the right side yielded several dual inhibitors with low nanomolar inhibition potencies on both human FAAH and human sEH enzymes. Modifications of the *meta* and *para* positions with the same groups led to a loss of inhibition potency towards the FAAH enzyme. On the other hand, the *ortho/para* di-substitutions were well-tolerated on both enzymes, and several potent dual inhibitors were identified with low nanomolar activity comparable to the *ortho-* substitution inhibitors. In this work, we followed up on these SAR studies and further explore the optimal substituent on the right side for dual sEH/FAAH inhibition. First, the effects of the placement of the electron-withdrawing and deactivating groups, trifluoromethyl- and cyano-, were examined in the *ortho* position of the aromatic ring, by designing **7a** and **7b**, respectively, Table 1. Next, the effects of placing the trifluoromethyl- group in the *meta* (**7c**) and *para* (**7d**) positions were tested on the dual inhibition potency. In addition, we were particularly interested in the trifluoromethyl group and placement of fluorine groups at various positions since, in our previous work[27], we substituted an H atom with an F atom to investigate how this specific change affects metabolic stability and activity. This isostere of H significantly improved liver microsomes half-lives and did not affect the activity. It also increased microsomal stability, especially when substitution occurred on the aromatic ring on the right side of the inhibitors. This suggests that this moiety is probably involved in the initial degradative process. Thus, fluorine atoms were introduced at specific positions of the right-side portion of the dual inhibitors, Fig. 3. Next, to elucidate the effect of another strongly electron-withdrawing group in the *para* position, we designed analog **7e** with the nitro-group. The rationale for designing the following three analogs, **7f**-**h**, was guided by the same rationale above; the chloro- or bromo- groups were kept in the *ortho* position since that was previously shown to be essential for the low nanomolar inhibition potencies on the both human FAAH and human sEH, while fluoro- or trifluoromethyl- groups were placed in the *para* position, to improve metabolic stability of the molecules. To elucidate the effects of di-substitution in the meta position of the activity with chloro- and bromo- groups, analog **7i** was designed, while for the effects of the meta disubstitution with trifluoromethyl- groups, analog **7j** was designed. Finally, the trisubstituted analog **7k** was intended to explore whether the activity

will be changed by the placement of chloro- groups in positions 2 and 6 and the bromo-group in position 4 on the aromatic ring.

The rational design of the new analogs included preliminary pharmacokinetic and pharmacodynamic predictions, Table 2. First, the oral bioavailability of the dual inhibitor **4** and newly designed compounds **7a-k** were predicted. According to *Lipinski Rule of 5*, logP values above 5, molecular weight (MW) above 500, number of hydrogen bond acceptors (HBA) above ten, and the number of hydrogen bond donors (HBD) above five usually mean poor absorption and low oral bioavailability.[32] All synthesized analogs in this study, **5a-k**, including the lead dual inhibitor **4**, are in agreement with the Lipinski Rule of 5 in terms of the number of hydrogen bond acceptors and the number of hydrogen bond donors. However, all analogs have molecular weights above 500 g/mol and logP above 5. On the other hand, according to Veber's Rule, another predictor of oral bioavailability, all synthesized analogs should possess good bioavailability after oral applications. This rule states that drug candidates will have good oral bioavailability if the polar surface area (PSA) of the drug is less than 140 Å and the number of rotatable bonds (RotB) present in a molecule is less than 10.[33] A full pharmacokinetic evaluation of these new compounds are needed to determine the exact oral bioavailability. Next, to evaluate absorption potential, the permeability efficacy was calculated. Typically, in the drug discovery process, two assays are used to determine the permeability of the drug candidates: Parallel Artificial Membrane Permeability Assay (PAMPA) and Caco-2 Permeability Assay. The software predicts permeability in both assays and provides the scores in cm/sec. A value above −5 indicates high permeability, and below −6 indicates low permeability. According to the calculated values (Table 2), all designed analogs would have moderate permeability in the Caco-2 assay and high permeability in PAMPA.[34, 35] In this work, the microsomal liver stability assay of the lead compound **4** was also evaluated (See section 2.3). We wanted to see how predicted values compare to the *in vitro* experiments; thus, we predicted half-life in human microsomes (HM $t_{1/2}$) for **4** and all other designed analogs. Based on the predicted values (given in minutes), analogs with fluoro- groups had slightly higher stability than **4** and other analogs. Finally, we calculated LD_{50}, Tox Score, and hERG inhibition as part of toxicity predictions. For LD_{50}, values below 0 indicate 1mg/kg - high toxicity, while values of 2 and above indicates 100mg/kg - low toxicity. Most of the designed analogs had values close to or above 2, indicating moderate to low toxicity. Tox Score prediction evaluates the possible toxicity based on the overall chemical structure or substituents known for potential toxicity. Values above 1 indicate a structure or substituent flagged as unfavorable, and values above 0.5 indicate a toxic compound. Only the analog **7e** (with the nitro group present in the *para* position) had a Tox Score of 0.5. Evaluating drug candidates for hERG inhibition became a standard procedure during the drug development process[36], thus, hERG inhibition was predicted, and according to the software, a value above 0.5 indicates a high probability of a drug being an hERG inhibitor. None of the designed analogs in this study had a value above 0.5.

The lead compound **4**, and analogs **7a-k**, were synthesized according to the previously established procedures[25], described in Scheme 1. The commercially available 2-(4-aminophenyl)benzothiazole and *N*-Boc-4-piperidine carboxylic acid were condensed via a coupling reaction with EDC and microwave irradiation. Next, amide **5** was subjected

to Boc-deprotection with trifluoroacetic acid (TFA), which provided the key intermediate **6**. Compound **6** was subsequently coupled with different R-benzenesulfonyl chlorides and microwave irradiation yielding compounds **7a-k** in moderate yields (40–71%).

The structures and purity of the final compounds were characterized by proton and carbon NMR spectroscopy (See Supplemental Information) and high-resolution mass spectrometry (HRMS).

3.2 Biological Evaluation

The lead compound **4** and the new benzothiazole-phenyl analogs **7a-k** were first evaluated *in vitro* in human sEH and human FAAH inhibition assays, Table 1. The analog **7a** with the electron-withdrawing trifluoromethyl group placed in the *ortho* position showed inhibition potency in the low nanomolar range for both human FAAH (IC_{50} = 9.7 nM) and human sEH (IC_{50} = 3.1 nM) enzymes. This was also the most potent benzothiazole-phenyl-based dual inhibitor identified in this series of analogs. Previously, we showed that placement of fluoro-, chloro- or methyl- groups in the *ortho* position led to very potent inhibitors of FAAH, with IC_{50} values of 1.3 nM, 7 nM and 9.6 nM, respectively, but showed lower activity for sEH, with IC_{50} value of 150 nM for fluoro- group, and high potencies for chloro- and methyl- groups with IC_{50} values of 9.6 nM and 35 nM.[25] Surprisingly, trifluoromethyl group in the *ortho* position (analog 7a) led to high potencies for both enzymes, illustrating complex impact of halogen and alkyl substituents in the binding pocket of sEH. On the other hand, the nitrile- group in the same position, **7b**, was well tolerated in the human sEH (IC_{50} = 19.5 nM) but was less potent for human FAAH (IC_{50} = 286.6 nM). Placement of the same trifluoromethyl- group in the *meta*, **7c** and *para*, **7d** led to moderate inhibition potencies at both enzymes. The nitro group placed in the *para* position, **7e** led to a complete loss of potency towards FAAH (IC_{50} > 10,000 nM) relative to the lead dual inhibitor **4**, and moderate potency at human sEH (IC_{50} = 363.9 nM), suggesting that polar strong electron-withdrawing groups are not favored in the active site of FAAH. Placing chloro-group in the *ortho* position and fluoro- group in the *para* position, **7f** led to high potencies for both enzymes, sEH (IC_{50} = 16.9 nM) and FAAH (IC_{50} = 19.1 nM). However, placement of chloro- in the *ortho* and bulkier trifluoromethyl- group in the *para* position, **7g**, was well tolerated in the FAAH (IC_{50} = 26.6 nM) but led to low potency for sEH (IC_{50} = 432.1 nM). The introduction of bromo- and fluoro- groups in the *ortho* and *para* positions, respectively, led to equally high potencies for both enzymes, with an IC_{50} value of 28.9 nM for FAAH and IC_{50} = 8.2 nM for human sEH. Next, the introduction of chloro- and bromo- in the *meta* positions, **7i**, led to discovering the disubstituted dual inhibitor with high potency at both enzymes comparable to the lead compound, having IC_{50} = 12.3 nM and IC_{50} = 17.0 nM for FAAH and sEH respectively. This analog was the second most potent dual inhibitor identified in this study, and again, suggesting that halogen groups (specifically the chloro-group) are well tolerated and favored by both enzymes. Di-substitution in the *meta* positions with the trifluoromethyl groups, **7j** led to good potency at FAAH (IC_{50} = 41.9 nM), but showed low micromolar inhibition for sEH (IC_{50} = 4837.5 nM). Finally, the trisubstituted analog, **7k**, showed good nanomolar potencies for both enzymes, with IC_{50} values of 89.7 nM for FAAH and 41 for sEH.

Since the best dual inhibitor(s) will be evaluated in animal models first, **4** and all newly synthesized analogs were also tested against the rat and mouse sEH to identify the best compound to use in a rodent model, Table 1. Previously, some urea-based sEH inhibitors were found less potent on rat and mouse sEH compared to their potency on the human enzyme.[37] Varying potencies on rat/mouse vs. human enzymes may have tremendous implications for the safety and utility of the dual inhibitor as an effective treatment for pain. Here, most dual inhibitors were significantly less potent on the mouse sEH enzyme than their potencies on human and rat enzymes. The sequence alignment of human, mouse, and rat enzymes shows high sequence similarity and contains many conserved amino acid residues located in the catalytic site of sEH (Figure S1); thus, the species selectivity might be due to the different shapes of active sites and binding modes of analogs. Nonetheless, these findings indicate that modeling pain and other behaviors in rats are the best model to evaluate these dual inhibitors given the similar potencies at inhibiting both rat and human sEH enzymes.

The lead compound **4** and the most potent compound identified in this study **7a** were selected for profiling in human, mouse, and rat microsomal liver assays (MLA). As shown in Table 3, both tested compounds showed poor metabolic profiles in human, mouse, and rat MLA. Previously, the introduction of an isosteric fluoro- group instead of a hydrogen atom significantly improved liver microsomes half-lives while it did not affect the activity.[27] However, this medicinal chemistry approach is not universally applicable, and did not apply to the benzothiazole-phenyl scaffold. In the future work, alternative known approaches, e.g., the inclusion of deuterium atom, modifying labile functional groups, and deactivating aromatic rings to improve the microsomal stability, which is a good predictor of *in vivo* metabolism and is an important tool in drug development should be tested to increase stability.

3.3 Molecular Modeling

Previously crystallographic data showed that amino acid residues Y383, Y466, and D335 are important for the sEH catalytic activity.[1, 31] On the other hand, the X-ray crystallographic structure of the rat FAAH in the complex with the inhibitor shows that three amino acid residues, K142, S217, and S241 are involved in the catalytic activity of this enzyme.[38, 39] Here, we wanted to determine whether the new analogs, **7a-k** bind similar to other amide-based sEH and FAAH inhibitors. Using ICM Pro software, docking experiments were performed in the human FAAH homology model[21] and the human sEH model. Analogs **7a-k** were docked and docking scores were obtained (Table S1). The most potent benzenethiazole-phenyl dual inhibitor discovered in this study, **7a** was selected as a representative to analyze the binding properties of this series of compounds. The docking experiments in the human FAAH homology model revealed that the trifluoromethyl- group is located in the proximity of the catalytic triad amino acid residues S217 and S241, Figs. 4A and 4B. Examination of the **7a** in the binding pocket of FAAH showed several important hydrophobic interactions that probably contribute to the low nanomolar inhibition potency of this analog; π-π stacking of aromatic ring and F192, amide bond interacting with the F432, T488 and M436 and benzothiazole moiety surrounded with W531, L429 and L433. The complete list of amino acid residues with their respective distances from **7a** are listed

in Table S2. The visual inspection of the analog **7a** in the binding pocket of human sEH model confirmed that the amide bond is in the close proximity of Y383, Y466 and D335, and in addition forms a hydrogen bond with Y466 (Figs. 5A and 5B). The trifluoromethyl-group makes hydrophobic interactions with Y383, F387 and L428. The aromatic ring has π-π interactions with F267 and an important hydrophobic interaction with M419, while benzothiazole ring has several hydrophobic contacts with W336, M339 and M469 (Table S3).

3.4   *In vivo* evaluation of voluntary wheel running

Intraperitoneal administration of 1 mg/kg of **4** alleviated acute inflammatory pain produced by an injection of formalin in the hind paw of male rats (i.e., Formalin Test).[26] This finding is especially promising because this dose of dual inhibitor was as effective as a higher dose of ketoprofen, the traditional nonsteroidal anti-inflammatory drug. Compound **4** seems to produce pain relief by interrupting pro-inflammatory processes, which is consistent with the mechanisms of action of dual sEH/FAAH inhibition.

The Formalin Test relies on motor behavior.[40] Briefly, an injection of formalin in the hind paw produces licking and guarding behaviors of the injected paw.[40] In fact, many preclinical pain tests rely on motor behavior to determine the extent and magnitude of pain relief in animals. One potential problem is that a therapeutic could simply inhibit *any* behavior and still produce a "false positive" on a pain test.[41] Thus, it is crucial to evaluate the effects of **4** on voluntary motor behaviors such as wheel running in naïve uninjured animals to ensure that dual sEH/FAAH inhibitors do not produce adverse effects. Wheel running has been used to evaluate the effects of pain and measure any adverse effects associated with drug use (e.g., sedation).[41-43] Wheel running is particularly useful because it is a natural and voluntary behavior for rats with clear diurnal rhythms. Computerized running wheels were placed in the rat's home cage to measure wheel running for three hours following intraperitoneal injection of the effective dose of **4** (1 mg/kg) and a higher dose of **4** (3 mg/kg) to determine any potential dose-dependent toxicity. Control rats received vehicle (i.e., no drug). Fig. 6 shows wheel running activity for two hours after injection of **4**. The average level of running over the two hours, relative the rats' baseline levels of running prior to drug injection, was analyzed between groups. An analysis of variance revealed that vehicle nor any dose of **4** (1 or 3 mg/kg) depressed wheel running in rats for up to 2 hours following intraperitoneal injection ($F_{(2,33)} = 2.12$, $p = 0.14$; Fig 6).

This finding is especially important for future *in vivo* evaluation of dual inhibitors for pain, as it provides evidence that any pain-related behaviors inhibited by dual inhibitors is due to its antinociceptive effects and not non-specific effects on locomotor activity. For example, previous studies have demonstrated that while morphine can produce pain relief in male rats, these same doses of morphine impair activity due to sedative side effects.[42] The same effect has been demonstrated with phytocannabinoids such as Δ9-tetrahydrocannabinol in that while THC produces pain relief, higher doses impair activity.[43] Here, we demonstrate that 1 mg/kg **4** produces pain relief on the Formalin Test[26] but does not impair normal activity (Fig. 6). Importantly, a higher dose (3 mg/kg) of **4** also does not impair activity

in male rats suggesting that the therapeutic window of dual sEH/FAAH inhibitors may be wider than traditional analgesics (e.g., opioids).

The present studies using our previously described lead compound **4**[26], provide an initial proof of concept that doses of dual sEH/FAAH inhibitors that produce pain relief do not impair activity in rats. These same approaches can be used to determine if other dual inhibitors such as **7a** also impair activity in rats. However, initial studies must first identify doses of **7a** that produce pain relief in rat models of acute and chronic inflammatory pain to further determine its antinociceptive potential. Given that dual sEH/FAAH inhibition produces pain relief against acute inflammatory pain at low doses,[26] we hypothesize **7a** will also alleviate pain within a similar dose range. Once this dose range has been identified, we will further examine potential side effects associated with therapeutic and supratherapeutic doses of **7a** and our other lead dual inhibitors to better understand the analgesic potential of dual sEH/FAAH inhibition.

4   Conclusion

This study is a follow-up SAR study of benzothiazole-phenyl analogs as potential dual inhibitors of FAAH and sEH enzymes. Strong nonpolar electron-withdrawing groups placed in *ortho* and/or in *ortho/para* positions are well-tolerated and were able to identify several potent dual inhibitors. The most potent inhibitor **7a**, with trifluoromethyl- group in the ortho position has an IC_{50} value of 9.7 nM for FAAH and $IC_{50} = 3.1$ nM for human sEH enzyme. All analogs were also screened against mouse and rat sEH inhibition assays, surprisingly, the new compounds were not active on mouse sEH. This prompt us to plan our future *in vivo* studies in rat models of pain. As a part of our preliminary pharmacokinetic studies, microsomal liver stability assay was performed on our lead dual inhibitor **4** and the best compound identified in this study **7a**. Although both compounds have similar comparable activity on both enzymes, we expected that **7a** will have better stability profile in liver microsomes based on our previous discoveries that fluorine groups placed on the aromatic ring increase stability. However, both dual inhibitors showed similar and short half-lives and in the future experiments other medicinal chemistry strategies should be tested to increase the half-life of this series of analogs. Molecular modeling experiments revealed that **7a** binds in the proximity of catalytic site of both sEH and FAAH models which contributes to the excellent inhibition profile of this analog. Lastly, *in vivo* evaluation determined that therapeutic and supra-therapeutic doses of **4** do not impair activity, suggesting that this novel strategy of dual sEH/FAAH inhibition may be a safe and effective approach to treat pain.

Supplementary Material

Refer to Web version on PubMed Central for supplementary material.

Acknowledgments

References

1. Imig JD; Hammock BD, Soluble epoxide hydrolase as a therapeutic target for cardiovascular diseases. Nat Rev Drug Discov 2009, 8 (10), 794–805. [PubMed: 19794443]

2. Morisseau C; Hammock BD, Impact of soluble epoxide hydrolase and epoxyeicosanoids on human health. Annu Rev Pharmacol Toxicol 2013, 53, 37–58. [PubMed: 23020295]

3. Kodani SD; Morisseau C, Role of epoxy-fatty acids and epoxide hydrolases in the pathology of neuro-inflammation. Biochimie 2019, 159, 59–65. [PubMed: 30716359]

4. Schmelzer KR; Kubala L; Newman JW; Kim IH; Eiserich JP; Hammock BD, Soluble epoxide hydrolase is a therapeutic target for acute inflammation. Proc Natl Acad Sci U S A 2005, 102 (28), 9772–7. [PubMed: 15994227]

5. Yang T; Peng R; Guo Y; Shen L; Zhao S; Xu D, The role of 14,15-dihydroxyeicosatrienoic acid levels in inflammation and its relationship to lipoproteins. Lipids Health Dis 2013, 12, 151. [PubMed: 24148690]

6. Wagner KM; McReynolds CB; Schmidt WK; Hammock BD, Soluble epoxide hydrolase as a therapeutic target for pain, inflammatory and neurodegenerative diseases. Pharmacol Ther 2017, 180, 62–76. [PubMed: 28642117]

7. Node K; Huo Y; Ruan X; Yang B; Spiecker M; Ley K; Zeldin DC; Liao JK, Anti-inflammatory properties of cytochrome P450 epoxygenase-derived eicosanoids. Science 1999, 285 (5431), 1276–9. [PubMed: 10455056]

8. Shen HC, Soluble epoxide hydrolase inhibitors: a patent review. Expert Opin Ther Pat 2010, 20 (7), 941–56. [PubMed: 20429668]

9. Pecic S; Deng SX; Morisseau C; Hammock BD; Landry DW, Design, synthesis and evaluation of non-urea inhibitors of soluble epoxide hydrolase. Bioorg Med Chem Lett 2012, 22 (1), 601–5. [PubMed: 22079754]

10. Shen HC; Hammock BD, Discovery of inhibitors of soluble epoxide hydrolase: a target with multiple potential therapeutic indications. Journal of medicinal chemistry 2012, 55 (5), 1789–1808. [PubMed: 22168898]

11. Shen HC; Ding FX; Deng Q; Xu S; Tong X; Zhang X; Chen Y; Zhou G; Pai LY; Alonso-Galicia M; Roy S; Zhang B; Tata JR; Berger JP; Colletti SL, A strategy of employing aminoheterocycles as amide mimics to identify novel, potent and bioavailable soluble epoxide hydrolase inhibitors. Bioorg Med Chem Lett 2009, 19 (19), 5716–21. [PubMed: 19700315]

12. Devane WA; Hanus L; Breuer A; Pertwee RG; Stevenson LA; Griffin G; Gibson D; Mandelbaum A; Etinger A; Mechoulam R, Isolation and structure of a brain constituent that binds to the cannabinoid receptor. Science 1992, 258 (5090), 1946–9. [PubMed: 1470919]

13. Sugiura T; Waku K, 2-Arachidonoylglycerol and the cannabinoid receptors. Chem Phys Lipids 2000, 108 (1-2), 89–106. [PubMed: 11106784]

14. Di Marzo V; Bisogno T; De Petrocellis L, Endocannabinoids and Related Compounds: Walking Back and Forth between Plant Natural Products and Animal Physiology. Chemistry & Biology 2007, 14 (7), 741–756. [PubMed: 17656311]

15. Ahn K; Johnson DS; Cravatt BF, Fatty acid amide hydrolase as a potential therapeutic target for the treatment of pain and CNS disorders. Expert Opin Drug Discov 2009, 4 (7), 763–784. [PubMed: 20544003]

16. Schmidt ME; Liebowitz MR; Stein MB; Grunfeld J; Van Hove I; Simmons WK; Van Der Ark P; Palmer JA; Saad ZS; Pemberton DJ; Van Nueten L; Drevets WC, The effects of inhibition of fatty acid amide hydrolase (FAAH) by JNJ-42165279 in social anxiety disorder: a double-blind, randomized, placebo-controlled proof-of-concept study. Neuropsychopharmacology 2021, 46 (5), 1004–1010. [PubMed: 33070154]

17. Griebel G; Stemmelin J; Lopez-Grancha M; Fauchey V; Slowinski F; Pichat P; Dargazanli G; Abouabdellah A; Cohen C; Bergis OE, The selective reversible FAAH inhibitor, SSR411298,

restores the development of maladaptive behaviors to acute and chronic stress in rodents. Scientific Reports 2018, 8 (1), 2416. [PubMed: 29403000]

18. Russo R; Loverme J; La Rana G; Compton TR; Parrott J; Duranti A; Tontini A; Mor M; Tarzia G; Calignano A; Piomelli D, The fatty acid amide hydrolase inhibitor URB597 (cyclohexylcarbamic acid 3'-carbamoylbiphenyl-3-yl ester) reduces neuropathic pain after oral administration in mice. J Pharmacol Exp Ther 2007, 322 (1), 236–242. [PubMed: 17412883]

19. Holt S; Comelli F; Costa B; Fowler CJ, Inhibitors of fatty acid amide hydrolase reduce carrageenan-induced hind paw inflammation in pentobarbital-treated mice: comparison with indomethacin and possible involvement of cannabinoid receptors. Br J Pharmacol 2005, 146 (3), 467–476. [PubMed: 16100529]

20. Wang Y; Zhang X, FAAH inhibition produces antidepressant-like efforts of mice to acute stress via synaptic long-term depression. Behav Brain Res 2017, 324, 138–145. [PubMed: 28193523]

21. Wilt SR; Rodriguez M; Le TNH; Baltodano EV; Salas A; Pecic S, Design, microwave-assisted synthesis, biological evaluation and molecular modeling studies of 4-phenylthiazoles as potent fatty acid amide hydrolase inhibitors. Chem Biol Drug Des 2020, 95 (5), 534–547. [PubMed: 32061147]

22. Sasso O; Wagner K; Morisseau C; Inceoglu B; Hammock BD; Piomelli D, Peripheral FAAH and soluble epoxide hydrolase inhibitors are synergistically antinociceptive. Pharmacological research 2015, 97, 7–15. [PubMed: 25882247]

23. Proschak E; Stark H; Merk D, Polypharmacology by Design: A Medicinal Chemist's Perspective on Multitargeting Compounds. J Med Chem 2019, 62 (2), 420–444. [PubMed: 30035545]

24. Anighoro A; Bajorath J; Rastelli G, Polypharmacology: Challenges and Opportunities in Drug Discovery. Journal of Medicinal Chemistry 2014, 57 (19), 7874–7887. [PubMed: 24946140]

25. Wilt S; Kodani S; Le TNH; Nguyen L; Vo N; Ly T; Rodriguez M; Hudson PK; Morisseau C; Hammock BD; Pecic S, Development of multitarget inhibitors for the treatment of pain: Design, synthesis, biological evaluation and molecular modeling studies. Bioorg Chem 2020, 103, 104165. [PubMed: 32891856]

26. Wilt S; Kodani S; Valencia L; Hudson PK; Sanchez S; Quintana T; Morisseau C; Hammock BD; Kandasamy R; Pecic S, Further exploration of the structure-activity relationship of dual soluble epoxide hydrolase/fatty acid amide hydrolase inhibitors. Bioorg Med Chem 2021, 51, 116507. [PubMed: 34794001]

27. Pecic S; Zeki AA; Xu X; Jin GY; Zhang S; Kodani S; Halim M; Morisseau C; Hammock BD; Deng SX, Novel piperidine-derived amide sEH inhibitors as mediators of lipid metabolism with improved stability. Prostaglandins Other Lipid Mediat 2018, 136, 90–95. [PubMed: 29567338]

28. Cardozo T; Totrov M; Abagyan R, Homology modeling by the ICM method. Proteins 1995, 23 (3), 403–14. [PubMed: 8710833]

29. Abagyan R; Totrov M, Biased probability Monte Carlo conformational searches and electrostatic calculations for peptides and proteins. J Mol Biol 1994, 235 (3), 983–1002. [PubMed: 8289329]

30. Abagyan R; Totrov M; Kuznetsov D, ICM—A new method for protein modeling and design: Applications to docking and structure prediction from the distorted native conformation. Journal of Computational Chemistry 1994, 15 (5), 488–506.

31. Pecic S; Pakhomova S; Newcomer ME; Morisseau C; Hammock BD; Zhu Z; Rinderspacher A; Deng S-X, Synthesis and structure–activity relationship of piperidine-derived non-urea soluble epoxide hydrolase inhibitors. Bioorganic & Medicinal Chemistry Letters 2013, 23 (2), 417–421. [PubMed: 23237835]

32. Lipinski CA, Drug-like properties and the causes of poor solubility and poor permeability. J Pharmacol Toxicol Methods 2000, 44 (1), 235–49. [PubMed: 11274893]

33. Veber DF; Johnson SR; Cheng HY; Smith BR; Ward KW; Kopple KD, Molecular properties that influence the oral bioavailability of drug candidates. J Med Chem 2002, 45 (12), 2615–23. [PubMed: 12036371]

34. van Breemen RB; Li Y, Caco-2 cell permeability assays to measure drug absorption. Expert Opin Drug Metab Toxicol 2005, 1 (2), 175–85. [PubMed: 16922635]

35. Markovic BD; Vladimirov SM; Cudina OA; Odovic JV; Karljikovic-Rajic KD, A PAMPA assay as fast predictive model of passive human skin permeability of new synthesized corticosteroid C-21 esters. Molecules 2012, 17 (1), 480–91. [PubMed: 22222907]

36. Garrido A; Lepailleur A; Mignani SM; Dallemagne P; Rochais C, hERG toxicity assessment: Useful guidelines for drug design. Eur J Med Chem 2020, 195, 112290. [PubMed: 32283295]

37. Kodani SD; Wan D; Wagner KM; Hwang SH; Morisseau C; Hammock BD, Design and Potency of Dual Soluble Epoxide Hydrolase/Fatty Acid Amide Hydrolase Inhibitors. ACS Omega 2018, 3 (10), 14076–14086. [PubMed: 30411058]

38. Ahn K; Johnson DS; Cravatt BF, Fatty acid amide hydrolase as a potential therapeutic target for the treatment of pain and CNS disorders. Expert Opin Drug Discov 2009, 4 (7), 763–784. [PubMed: 20544003]

39. Cravatt BF; Lichtman AH, Fatty acid amide hydrolase: an emerging therapeutic target in the endocannabinoid system. Curr Opin Chem Biol 2003, 7 (4), 469–75. [PubMed: 12941421]

40. Dubuisson D; Dennis SG, The formalin test: a quantitative study of the analgesic effects of morphine, meperidine, and brain stem stimulation in rats and cats. Pain 1977, 4 (2), 161–174. [PubMed: 564014]

41. Kandasamy R; Morgan MM, 'Reinventing the wheel' to advance the development of pain therapeutics. Behav Pharmacol 2021, 32 (2&3), 142–152. [PubMed: 33079736]

42. Kandasamy R; Calsbeek JJ; Morgan MM, Analysis of inflammation-induced depression of home cage wheel running in rats reveals the difference between opioid antinociception and restoration of function. Behav Brain Res 2017, 317, 502–507. [PubMed: 27746208]

43. Kandasamy R; Dawson CT; Craft RM; Morgan MM, Anti-migraine effect of (9)-tetrahydrocannabinol in the female rat. Eur J Pharmacol 2018, 818, 271–277. [PubMed: 29111112]
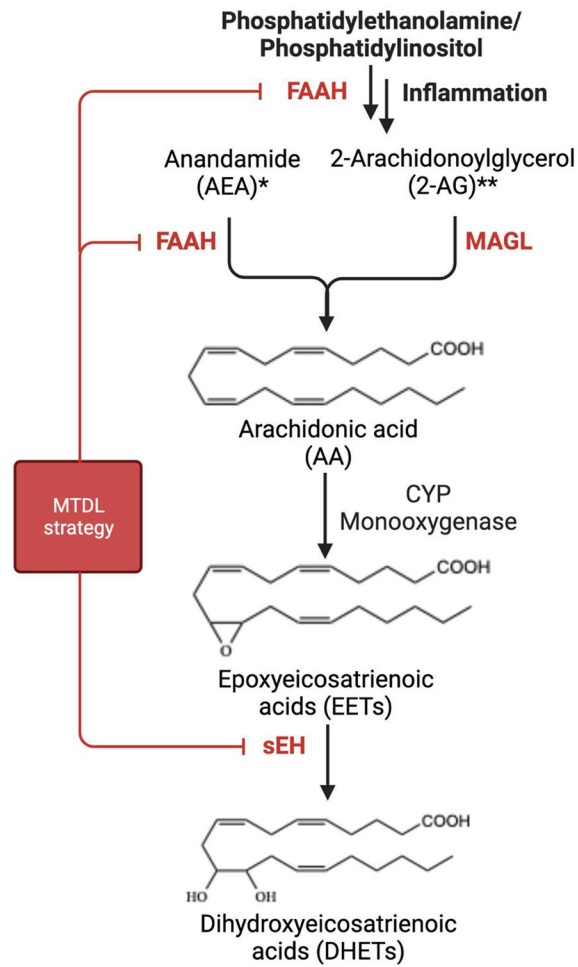
Figure 1.
Overview of the Arachidonic acid (AA) metabolism with FAAH and sEH.
*Degradation of AEA with FAAH will produce AA and ethanolamine.
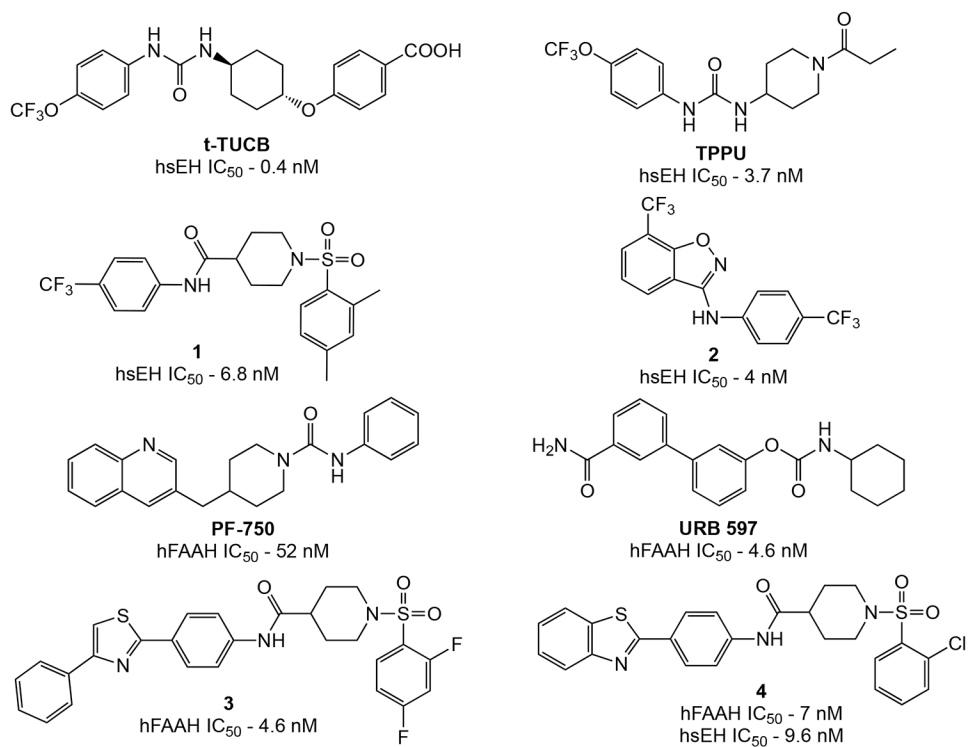**Degradation of 2-AG with FAAH will produce AA and glycerol.

Figure 2.
Chemical structures of known FAAH, sEH and dual sEH/FAAH inhibitors with their respective inhibition potencies.
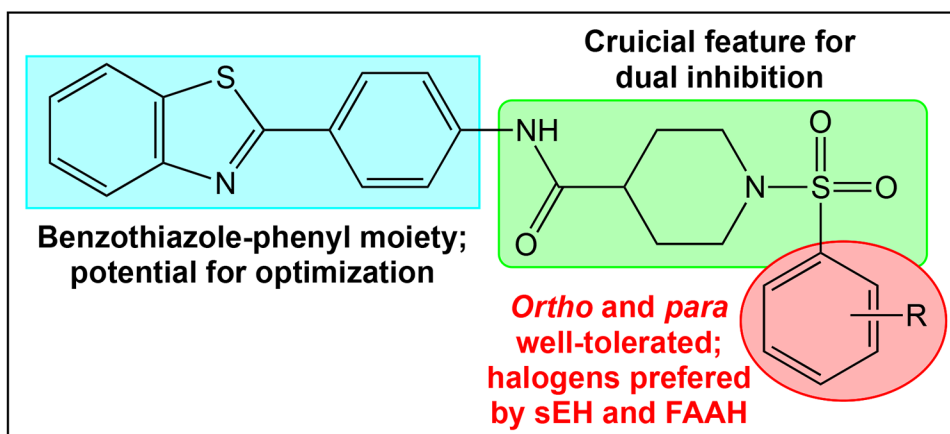
Figure 3.
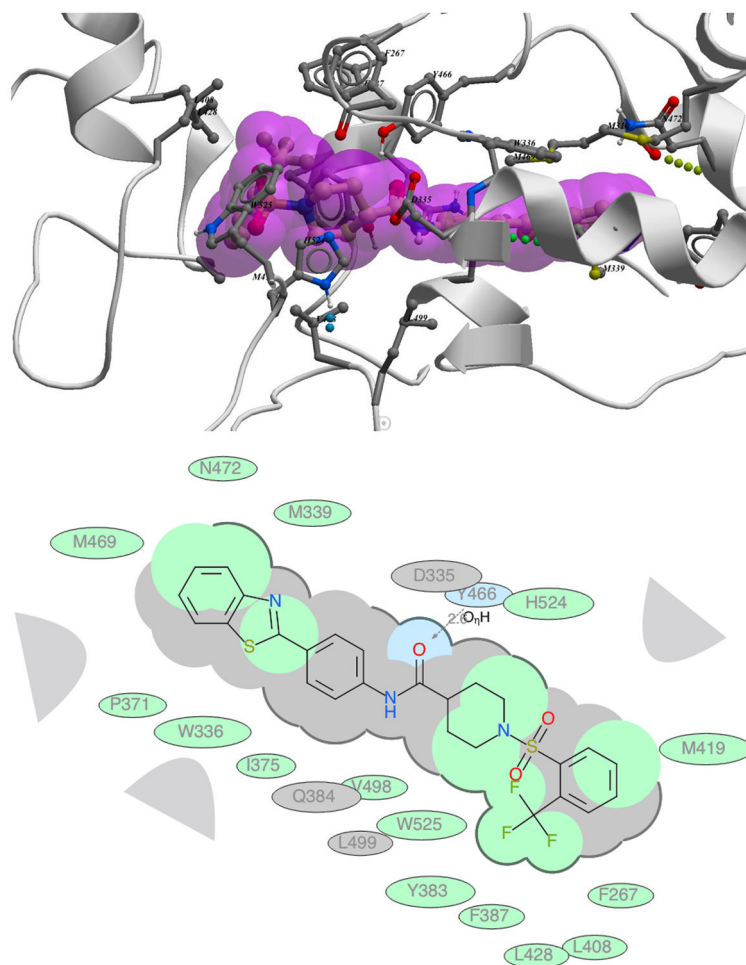SAR on the benzothiazole-phenyl dual inhibitors.

Figure 4.
Docking of **7a** in the human FAAH active site. **4A.** 3D representation: Amino acid residues in the proximity of **7a** are shown and labeled. **4B.** 2D representation: green shading represents hydrophobic regions; gray parabolas represent accessible surfaces for large areas; broken thick line around **7a** shape indicates accessible surfaces; size of residue ellipse represents the proximity to ligand, i.e. larger residue ellipse means closer to ligand and vice versa.
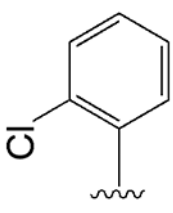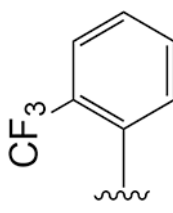
Figure 5.
Docking of **7a** in the human sEH active site. **5A.** 3D representation: Amino acid residues in the proximity of **7a** are shown and labeled. **5B.** 2D representation: green shading represents hydrophobic regions; gray parabolas represent accessible surfaces for large areas; gray dotted lines represent hydrogen bonds; broken thick line around **7a** shape indicates accessible surfaces; size of residue ellipse represents the proximity to ligand, i.e. larger residue ellipse means closer to ligand and vice versa.
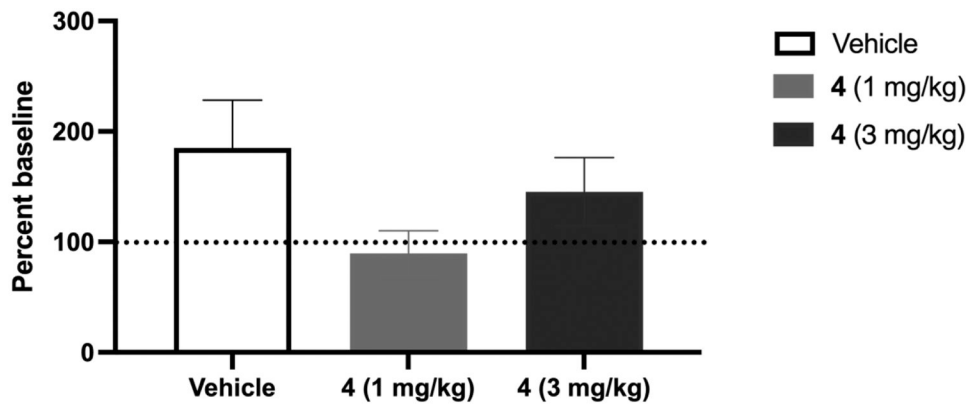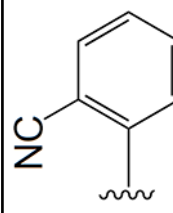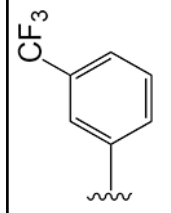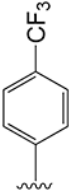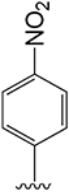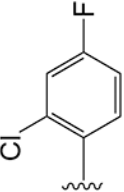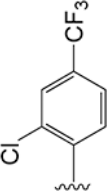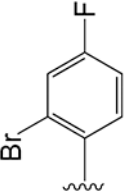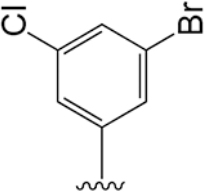
Figure 6.
Wheel running following injections of vehicle or **4**. Wheel running was measured for two hours following intraperitoneal injection of drug. The dotted line represents the rats' baseline levels of running. The running in the two hours following injection of drug is averaged and compared as a percent of the rat's baseline activity. Wheel running did not change between rats treated with vehicle or any dose of **4** ($p > 0.05$).
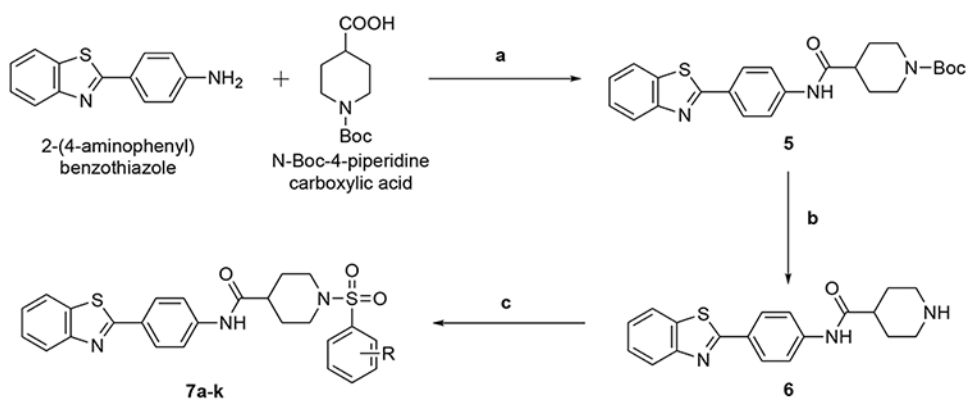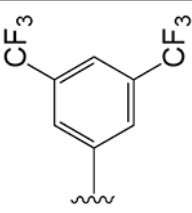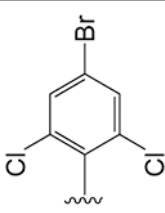
Scheme 1. Reagents and conditions:
(a) EDC, DMAP, DCM, 20 min, 80 °C, microwave irradiation, 76%; (b) TFA, DCM, 18 h, 90%; (c) R-benzenesulfonyl chloride (see Table 1 for R), Et$_3$N, DCM, 20 min, 80 °C, microwave irradiation, 40–71%.

TABLE 1.

Fatty acid amide hydrolase (FAAH) and soluble epoxide hydrolase (sEH) inhibitory activities

Compound	R	Human FAAH IC$_{50}$ (nM)	Human sEH IC$_{50}$ (nM)	Mouse sEH IC$_{50}$ (nM)	Rat sEH IC$_{50}$ (nM)
URB 597	-	38	-	-	-
t-TUCB	-	-	0.4	2.3	9.3
4	Cl	7.0	9.6	812.8	3.9
7a	CF$_3$	9.7	3.1	7,214.1	5.7
7b	NC	286.6	19.5	578.1	185.3
7c	CF$_3$	22.3	89.3	4,311.0	124.2

Compound	R	Human FAAH IC$_{50}$ (nM)	Human sEH IC$_{50}$ (nM)	Mouse sEH IC$_{50}$ (nM)	Rat sEH IC$_{50}$ (nM)
7d	CF$_3$	48.1	51.5	9,184.7	28.9
7e	NO$_2$	363.9	>10,000	>10000	4,478.5
7f	F, Cl	19.1	16.9	266.9	115.9
7g	CF$_3$, Cl	26.6	432.1	9,057.1	859.2
7h	F, Br	28.9	8.2	402.1	11.8
7i	Cl, Br	12.3	17.0	>10000	46.6

Compound	R	Human FAAH IC$_{50}$ (nM)	Human sEH IC$_{50}$ (nM)	Mouse sEH IC$_{50}$ (nM)	Rat sEH IC$_{50}$ (nM)
7j	(3,5-bis(CF$_3$)phenyl)	41.9	4837.5	>10000	2,906.3
7k	(4-Br-2,6-dichlorophenyl)	89.7	41.0	1,789.6	42.5
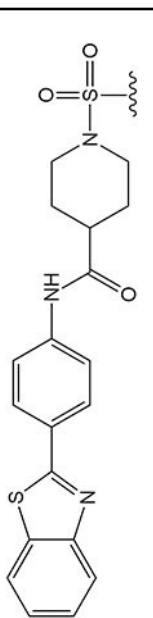
Table 2.

Predicted pharmacokinetic and pharmacodynamic properties for benzothiazole-phenyl dual sEH/FAAH inhibitors.

ID	MW	cLogP	HBA	HBD	PSA	RotB	Caco-2	PAMPA	HM t$_{1/2}$(min)	LD$_{50}$	Tox	hERG
URB 597	338.4070	4.10	5	3	66.14	6	−4.98	−5.06	23.1	1.70	2	0.21
t-TUCB	438.4032	5.22	7	3	74.19	9	−4.87	−5.18	115.2	2.64	0.8	0.06
4	512.0390	4.93	8	1	64.48	6	−5.24	−4.40	31.2	1.85	0	0.16
7a	545.5952	5.56	8	1	64.48	7	−5.18	−4.44	35.7	1.96	0	0.16
7b	502.6070	4.44	9	1	81.54	7	−5.23	−4.37	41.4	1.67	0	0.18
7c	545.5952	5.59	8	1	64.48	7	−5.22	−4.51	31.8	2.07	0	0.18
7d	545.5952	5.64	8	1	64.48	7	−5.23	−4.54	41.1	1.98	0	0.31
7e	522.5940	4.69	12	1	97.87	7	−5.25	−4.43	80.3	2.02	0.5	0.25
7f	530.0294	5.25	8	1	64.48	6	−5.37	−4.46	29.8	2.04	0	0.30
7g	580.0372	5.92	8	1	64.48	7	−5.34	−4.69	27.6	2.07	0	0.33
7h	574.4834	5.39	8	1	64.48	6	−5.38	−4.41	30.6	1.79	0	0.27
7i	590.9350	6.11	8	1	64.48	6	−5.39	−4.71	26.4	1.90	0	0.34
7j	613.5934	6.36	8	1	64.48	8	−5.32	−5.11	29.7	2.36	0	0.25
7k	625.3770	6.22	8	1	64.48	6	−5.43	−4.81	36.6	1.77	0	0.33

Table 3.

Metabolic stability of dual sEH/FAAH inhibitors against human, mouse and rat microsomes.

Compound	Species	Half-life^a (min)	CL_{int}^{b} (mL/min/mg protein)
4	Human	18.1	0.076
	Mouse	11.3	0.122
	Rat	8.82	0.157
7a	Human	24.0	0.057
	Mouse	15.8	0.087
	Rat	14.7	0.094
Testosterone (control)	Human	22.7 *	0.061
	Mouse	4.95 **	0.28
	Rat	1.10 ***	1.25

^{a}When the calculated half-life is < the first non-zero timepoint. Data represents averages of duplicate determination.

^{b}Intrinsic clearance (CL_{int}) was calculated based on $CL_{int} = k/P$, where k is the elimination rate constant and P is the protein concentration in the incubation.

* Acceptable Range ($t_{1/2}$, min): 41

** Acceptable Range ($t_{1/2}$, min): 15

*** Acceptable Range ($t_{1/2}$, min): 15